Characterization of the copper K x-ray emission profile: an *ab initio* multi-configuration Dirac–Hartree–Fock approach with Bayesian constraints

2016 J. Phys. B: At. Mol. Opt. Phys. 49 035601

(http://iopscience.iop.org/0953-4075/49/3/035601)

IOP Publishing Journal of Physics B: Atomic, Molecular and Optical Physics
J. Phys. B: At. Mol. Opt. Phys. **49** (2016) 035601 (14pp) doi:10.1088/0953-4075/49/3/035601

Characterization of the copper $K\beta$ x-ray emission profile: an *ab initio* multi-configuration Dirac–Hartree–Fock approach with Bayesian constraints

T LH Pham[1], T VB Nguyen[1], J A Lowe[1], I P Grant[2,3] and C T Chantler[1]

[1] School of Physics, The University of Melbourne, Australia
[2] Mathematical Institute, Andrew Wiles Building, Radcliffe Observatory Quarter, Woodstock Road, OX2 6GG, UK
[3] (DAMTP)—Department of Applied Mathematics and Theoretical Physics, Centre for Mathematical Sciences, Wilderforce Road, Cambridge, CB3 0WA, UK

E-mail: chantler@unimelb.edu.au

Received 5 October 2015, revised 29 October 2015
Accepted for publication 23 November 2015
Published 8 January 2016

Abstract

We investigate the $K\beta$ characteristic radiation and the complex asymmetric structure of photoemission lines of copper, which provides a benchmark for theoretical and experimental studies of x-ray calibration series in transition metals. *Ab initio* multi-configuration Dirac–Hartree–Fock (MCDHF) calculations have been performed to study the complex open-shell many-electron problem in copper. The biorthogonalization technique permits determination of transition intensities and Einstein A coefficients. The results from our MCDHF calculations demonstrate excellent convergence in transition energies and intensities, as well as gauge invariance to 0.6%. Shake processes caused by single and double spectator vacancies from 3d, 3p, 3s and 4s subshells have also been investigated extensively. MCDHF has been performed to calculate energies and relative intensities of 3d, $3d^2$, 3p, 3s and 4s satellites, resulting in the total number of configuration states exceeding 100 000 and more than 1500 transition components. Our theoretical calculations of shake-off probabilities using the multi-configuration method in the sudden limit have a high degree of internal consistency with the best available experimental data for copper $K\beta$. This supports the validity of relativistic atomic theory and sets a new benchmark even for poorly resolved characteristic spectra using current techniques of analysis.

Keywords: copper Kβ, MCDHF, characteristic radiation, shake processes

(Some figures may appear in colour only in the online journal)

1. Introduction

Discrete photoemission lines arise from bound–bound electron transitions in atoms. The $K\beta$ process is the transition from a $1s^{-1}$ state to a $3p^{-1}$ state followed by the spontaneous emission of an x-ray photon [1]. The notation $1s^{-1}$ and $3p^{-1}$ refers to a vacancy in the 1s and 3p subshells respectively as compared to the neutral atoms.

In order to determine the $K\beta$ spectrum, we perform multi-configuration Dirac–Hartree–Fock (MCDHF) calculations for the $3p^{-1}$ state. The electron configuration is assumed to be initially in the canonical $3d^{10}4s^1$ ($1s^2\ 2s^2\ 2p^6\ 3s^2\ 3p^5\ 3d^{10}\ 4s^1$) atomic ground state. In addition to the $1s^{-1} \rightarrow 3p^{-1}$ diagram transition, there are also processes known as shake-off and shake-up. Shake-off processes involve a second electron ionization into the continuum. The shake-up process involves an additional electron excited into the higher bound state.

High-accuracy theoretical studies of $K\alpha$ emission in copper has been presented in recent literature. Chantler *et al*

have successfully performed relativistic calculations to obtain the $K\alpha$ spectrum in excellent agreement with experiment, demonstrated well-converged wavefunctions and gauge invariance [2], and accounting for fine structure contribution to the spectrum, as well as offering reliable techniques for spectator vacancy modelling in the 3p, 3d and 4s subshells [3, 4].

The $K\beta$ emission spectrum, however, poses several challenges. The transition between $1s^{-1}$ and $3p^{-1}$ in fact involves six transition lines according to Fermi's golden rule for electric dipole transitions (E1): three transitions between $J = \{0, 1\}$ and $J = \{1, 2\}$ ($K\beta_1$), and three transitions between $J = \{0, 1\}$ and $J = \{0, 1\}$ ($K\beta_3$). The spectra of six $K\beta_{1,3}$ transitions and the additional transitions due to shake processes are strongly overlapping with each other. The total spectrum of the copper $K\beta$, as a result, is a single asymmetrical broad peak rather than two sharp peaks as with copper $K\alpha$. The deconvolution of the $K\beta$ spectrum of copper is more complicated and subject to several uncertainties. Moreover, discrepancies in the results of shake processes between theoretical and experimental literatures have been unresolved. Therefore, a high accuracy theory and more advanced technique are required to further understand the profile of copper $K\beta$ x-ray emission.

2. Theory

2.1. Multi-configuration Dirac-Hartree-Fock (MCDHF) method

MCDHF is based on the Dirac–Hartree–Fock (DHF) approach for many-electron atomic systems. Here, the atomic state functions (ASFs) are linear combinations of configuration state functions (CSFs) [3]:

$$\Psi(\Pi JM) = \sum_r c_r \Phi\left(\gamma_r \Pi JM\right) \tag{1}$$

$\Phi(\gamma_r \Pi JM)$ are linear combinations of Slater determinants, obtained from orthonormal Dirac spinors, with well-defined parity and angular momentum ΠJM, forming an orthonormal basis. γ_r includes all the quantum numbers necessary to define the unique electron configuration [5, 6]. Although using a single CSF gives a good approximation to the exact wavefunction, a linear combination of orthonormal CSFs offers even closer approximation. The mixing coefficients, c_r, can be obtained by diagonalizing of the Dirac–Coulomb Hamiltonian H_{DC}:

$$H_{\mathrm{DC}} = \sum_i^N \left(c\boldsymbol{\alpha_i}\cdot\boldsymbol{p_i} + V_{\mathrm{nucl}}(r_i) + \left(\beta_i - 1\right)c^2\right) + \sum_{i\geqslant j}^N \frac{1}{r_{ij}}. \tag{2}$$

In the MCDHF implementation of GRASP2K, the Breit interaction [7], QED corrections for self-energy and vacuum polarization, and finite nuclear mass effects are included perturbatively [8]. Each CSF in equation (1) is a wavefunction of the form:

$$\Phi_{E\kappa m}(\boldsymbol{r}) = \mathcal{A}\left[\prod_{i=1}^N \phi_{iE\kappa m}(\boldsymbol{r})\right],$$
$$\phi_{E\kappa m}(\boldsymbol{r}) = \frac{1}{r}\begin{pmatrix} P_{E\kappa}(r)\chi_{\kappa m}(\theta,\varphi) \\ \mathrm{i}Q_{E\kappa}(r)\chi_{-\kappa m}(\theta,\varphi)\end{pmatrix}, \tag{3}$$

where the two-component spin-orbit functions $\chi_{\kappa m}(\theta, \phi)$ include an amplitude and are simultaneously eigenfunctions of $\boldsymbol{j}^2$, $\boldsymbol{l}^2$ and $\boldsymbol{s}^2$. $\mathcal{A}$ is the antisymmetrization operator, and $P_{E\kappa}$ and $Q_{E\kappa}$ are the large and small components of the radial wavefunction. The angular-spin components $\chi_{\kappa m}(\theta, \phi)$ are orthonormal by design, and the overlap of the two wavefunctions can be evaluated as:

$$\left\langle \phi^*_{E'\kappa'm'} \middle| \phi_{E\kappa m} \right\rangle = \int_0^\infty \left(P_{E'\kappa'}(r)P_{E\kappa}(r) + Q_{E'\kappa'}Q_{E\kappa}(r)\right)\mathrm{d}r. \tag{4}$$

The orthonormality condition from equation (4) gives:

$$\left\langle \phi^*_{E'\kappa'm'} \middle| \phi_{E\kappa m} \right\rangle = \delta_{E,E'}\delta_{\kappa\kappa'}. \tag{5}$$

2.2. Photoionization and the shake processes

When inner-shell photoionization occurs, an inner-shell hole is created, and an electron is ionized. In this study, as is conventional, we assume that the shake-off process is dominant, while shake-up processes are considered negligible. The validity of this assumption is strongly supported in the literature, and the details will be provided in section 7.1. The shake-off process can also be explained as a result of a sudden change in effective nuclear charge 'seen' by the atomic electrons [9]. Shake-off processes are observed in photoemission, x-ray absorption fine structure and x-ray absorption near-edge structure [10, 11]. Due to a sudden removal of some electrons on the outer shells, there are additional transitions which strongly overlap with the diagram lines. These satellites blend with the diagram lines, yielding a broad asymmetric peak.

3. Theoretical calculations of copper $K\beta$ diagram lines

3.1. Copper $K\beta$ using Dirac–Fock (DF) and Hartree–Fock (HF) methods (Deutsch et al 1995)

The spectra of copper $K\alpha$ and $K\beta$ were recently measured with double and single crystal diffractometers using high precision techniques [12]. Atomic structure calculations were also done by Deutsch *et al* [12], using the relativistic DF code GRASP92 [6] and the non-relativistic HF code HF86 [13]. In the calculations, the initial and final state wavefunctions were generated in separate single configuration runs, where the orbital wavefunctions and energies were allowed to vary.

These results [12, 14] are excellent and highly illuminating. However, due to limitations of available computational

techniques, several assumptions were made to make the calculations manageable. The most significant simplifying assumption is that the single electron in the 4s subshell of the copper atom was neglected in all calculations. This reduces the open-shell copper system to a closed-shell system, increasing convergence and stability significantly. However, by omitting the 4s electron, they were not able to obtain the convergence to the eigenenergies. The theoretically calculated energies had to be shifted to align to with the experimental values. Furthermore, reducing the problem to a closed shell system may pose some non-negligible effects on the system since all fine-structure has been eliminated. In addition, the transition energies for the various lines were calculated by taking the difference in energy of pairs of levels from separate runs, as allowed by electric dipole moments and as required by the available computational tools.

This approach provides a logical means for calculating the relative transition probabilities within a multiplet, but requires two non-orthogonal basis sets to be transformed into a single orthogonal set, which was not available in GRASP92. Therefore, only transition energies were reported [12]. Other transition data such as intensities and radiative rates of transitions were not calculated.

3.2. Our method—MCDHF using the computational package GRASP2K 1.1 with RCI4

The calculations in this study were carried out using GRASP2K version 1.1 with RCI4, the revised version of GRASP2K v.1.0 and v.1.1—a fully relativistic, multi-configuration atomic structure package. One of the most important improvements in our method compared to all previous works is that advanced transition code has been implemented in GRASP2K v.1.0 [15]. A biorthogonal transformation scheme in biotra permits the use of initial and final states with different orbital sets. The enlargement of the basis sets for initial and final states separately makes for more rapid convergence of their properties, stabilizing the transition energy, and the use of separately optimized expressions also speeds up the convergence of the calculation of oscillator strengths, Einstein *A*-coefficients and gf-values. The latest version of GRASP2K, together with our theoretical models, permit well-converged DF wavefunctions.

Furthermore, the calculation of electron self-energy based on the LCG-Welton method in version 1.1 of GRASP2K, RCI4 (Nguyen *et al* 2015) [16] has also be implemented. The effects of finite-nuclear-size is also included in the calculations of electron self-energy. The calculations of $K\beta$ transitions in copper can now be done with higher level of accuracy.

In our calculations, the electron in the 4s shell is now included explicitly. This open-shell orbital adds a level of difficulty to the calculations, but provides higher potential accuracy. The total J quantum numbers are now included correctly according to the electronic configurations of the initial and final states, and the multiplicities are therefore different from the values from Deutsch *et al* [12]. The sets of J values of the initial and final states for [12] were $\left\{\frac{1}{2}\right\}$ and $\left\{\frac{1}{2}, \frac{3}{2}\right\}$ respectively. In this case, the number of electric dipole transitions ($E1$) according is two, namely $J = \frac{1}{2} \rightarrow J = \frac{1}{2}$ (β_3) and $J = \frac{1}{2} \rightarrow J = \frac{3}{2}$ (β_1). The multiplicity is $2J + 1$, hence the relative strength of the transitions between β_3 and β_1 is about 1:2 as expected from the multiplicity of the upper state. If the 4s shell is taken into account, the set of J angular quantum numbers for the initial state is $\{0, 1\}$, and the set of J for the final state is $\{0, 1, 1, 2\}$.

4. $K\beta$ diagram line calculations using GRASP2K 1.1, RCI4

We use GRASP2K 1.1, RCI4, with the method of valence–valence correlation. The reference configuration is divided into two regions—a set of 'core' orbitals, which consists of electrons in the 1s, 2s and 2p subshells, and the remainder is included in the 'active' set. Our process is iterative, such that at each stage of the calculation, the active set is expanded to include additional correlation orbitals. The process of building up the initial and final states of copper is as follows: first all the spectroscopic orbital wavefunctions of 1s, 2s, 2p, 3s, 3p 3d and 4s are optimized. Then the spectroscopic orbitals are frozen, which means that these orbitals are no longer optimized. CSFs are generated, and the 'active' set of orbitals, including 3s, 3p, 3d and 4s, are then expanded up to 4f and to 5s respectively. Single and double excitations are permitted only within the active set, but no core-valence or core-core correlation is included. The optimum approach to convergence is dependent on the system. Increasing the active set to include 1s, 2s and 2p orbitals increases the number of CSFs dramatically and makes convergence much more difficult, but does not change the results in our test investigations significantly so long as the wavefunction converges [3].

4.1. Method 1—default ordering and correct angular momenta range

Here we restrict the maximum total angular momentum number Js to be the exact values as calculated from the configuration. In particular, for $n \geqslant 4$, J takes the values of $\{0, 1\}$ for the initial states and $\{0, 1, 2\}$ for the final state. The number of transitions now is also restricted to 6, as we expect from the Fermigolden rule for electric dipole transitions (E1).

This method was introduced in the GRASP2K manual [17]. It was used in the relativistic calculations for copper $K\alpha$ [3, 4], titanium $K\alpha$ [18], for the 557.7 nm and 297.2 nm emission lines in oxygen [19] and for the transitions in O(I) and O(III) [20].

Table 1. Results of the $K\beta$ transitions in copper from the relativistic atomic calculations using method 1 and method 2.

Method	Expansion	Energy (eV)	β_3 A^L/A^V	gf total	Energy (eV)	β_1 A^L/A^V	gf total	WMLP (eV)	gf ratio (β_3: β_1)	Separation (eV)
1	5s	8899.80	1.0065	0.0475	8902.42	1.0062	0.0930	8901.54	0.5106	2.62
2	No	8900.38	1.0066	0.0476	8902.89	1.0063	0.0931	8902.02	0.5107	2.56
	4s	8900.35	1.0066	0.0475	8902.90	1.0063	0.0930	8902.04	0.5103	2.55
	4f	8900.68	1.0065	0.0473	8903.23	1.0064	0.0926	8902.37	0.5107	2.56
	5s	8900.67	1.0065	0.0473	8903.22	1.0064	0.0926	8902.36	0.5107	2.56

Gauge convergence is within 0.65% and the component ratio is convergent to the fourth significant figure. The weighted mean line position (WMLP) is calculated from the transition energies and their corresponding intensities.

4.2. Method 2—addressing the correct CSFs with dominant contributions to the total ASF

After building up the atomic configuration, we have a list of CSFs with the same J and parity in each block. Each CSF is indicated by an ASF serial number based on its order in the block. The multi-configuration expansion permits single and double excitations, allowing for thousands of possibilities of extra configurations, each with very small contribution to the ASF. The dominant configurations that contribute to the true wavefunction are the configurations in each block prior to the expansion, denoted by the ASF serial numbers.

In method 2, we must check the output of GRASP2K to ensure the CSFs with dominant contributions to the ASF are indicated correctly in each block. In theory the values of ASF serial numbers should not change with the multi-configuration expansion. However, by checking the configuration state list (CSL), we notice that some of the CSFs have been re-ordered, and hence, the original ASF serial numbers may no longer address the correct CSFs with dominant contributions to the ASF. Therefore, after expanding the basis set, we had to manually check the CSL and change the values of the ASF serial number according to the positions of the dominant contributing CSFs. Method 2 has been done solely by the authors, and has not been previously reported in the literature.

4.3. Discussion of methods

Both methods give plausible results in table 1, in comparison with the transition energies obtained using both DF and HF code [12, 14]. The number of transition lines using either method is consistent with the Fermi's golden rule for electric dipole transitions, retaining the qualitative fine structure correctly. The Babushkin gauge and Coulomb gauge in each transition are also convergent, with the ratios A^L/A^V very close to unity. The values of each transition energy, A^L and A^V and intensity after the multi-configuration expansion converge to a plausible value.

The results from method 2 are more reliable than those from method 1, since checking and manually re-ordering the CSL ensure the dominant CSFs are indicated correctly in the computation processes. Because the 3d and 4s orbitals lie very close to each other, as the multi-configuration expansion is applied and single and double excitations are allowed, the energy levels of these orbitals can be mixed, and some CSFs may have been re-ordered in the list. For this reason, method 2 is reflective of the physical CSFs and will be used for later calculations and analysis.

5. Stability and convergence of transition gauges, energies, peak separation and intensity (gf) ratios

For electric multipole transitions in the relativistic limit, the oscillator strengths can be calculated in two different gauges, Babushkin and Coulomb, which are the equivalents of the relativistic length and velocity gauges. The transition matrix elements depend on the choice of gauge. If wavefunctions were complete and exact then the transition elements would be gauge invariant. The ratios of the intensities calculated with Babushkin and Coulomb gauges (table 1) are all close to unity in both method 1 and method 2, within 0.65%. This is an indicator that the wavefunctions in our calculations are convergent.

The transition energies also converge to a plausible value in each method, implying a high level of convergence. The transition energies calculated here are consistent with theoretical results obtained by Deutsch *et al* [12].

The peak separation between β_3 and β_1 found by methods 1 and 2 are in good agreement with the theoretical results obtained by Huang *et al* [21] and by Deutsch *et al* [12], the experimental results by McAlister *et al* [22] and by Fuggle and Mårtensson [23] (table 2). The experimental result, however, has significant uncertainties. The uncertainties in our values of peak separation come from the convergence of transition energies after the multi-configuration expansion up to the 5s sub-shell. In other world, the uncertainties, $\delta(\Delta E)$, are evaluated as: $\delta(\Delta E) = \left(\Delta E_{5s} - \Delta E_{4f}\right)$. The intensity ratios we obtain from both methods are consistent with theoretical [24] and experimental literature [12, 25, 26]. Our convergence is to 0.01 eV peak separation and the fourth significant figure for the component ratio $\beta_3 : \beta_1$. Of course this is not a statement about accuracy.

Core–valence and core–core correlations make the calculations much more complicated due to the large number of CSFs; however, the peak separation and relative intensities are unchanged.

Table 2. Comparison of separation in literature and this work for copper $K\beta$.

	Source	Separation (eV)	gf ratio (β_3:β_1)
Experimental	Bearden and Shaw [27]	2.0 ± 0.1	N/A
(Semi-empirical)	McAlister *et al* [22]	2.0 ± 1.0	N/A
	Cuthill and Erickson [22]	2.4 ± N/A	N/A
	Madden *et al* [28]	2.7 ± N/A	0.63
	Bruhn *et al* [29]	2.25 ± 0.07	N/A
	LaVilla [25]	2.4 ± N/A	0.5
	Bremer *et al* [26]	2.2 ± 0.3	0.51
	Fuggle and Mårtensson [23]	2.2 ± 0.5	N/A
	Deutsch *et al* [12]	2.39 ± 0.02	0.51
Theoretical	Herman and Skillman [30]	2.7 ± N/A	N/A
	Huang *et al* [21]	2.55 ± N/A	N/A
	Misra *et al* [31]	2.49 ± N/A	N/A
	Scofield [24]	N/A	0.511
	Deutsch *et al* [12]	2.55 ± N/A	0.51
This work	Method 1	2.6209 ± 0.0066	0.5106
	Method 2	2.5561 ± 0.0102	0.5107

The experimental values are outputs from semi-empirical fits with or without deconvolution. N/A implies that the value is not available. The uncertainties of our peak separation values come from the convergence of the transition energies from the multi-configuration expansion up to the 5s subshell (see text). The peak separation using method 2 is consistent with the theoretical results obtained by Huang *et al* [21] and Deutsch *et al* [12]. Our intensity (gf) ratio between β_3 and β_1 also strongly agrees with most of the available values from theoretical and experimental literature by LaVilla [25], Bremer *et al* [26], Deutsch *et al* [12] and Scofield [24].

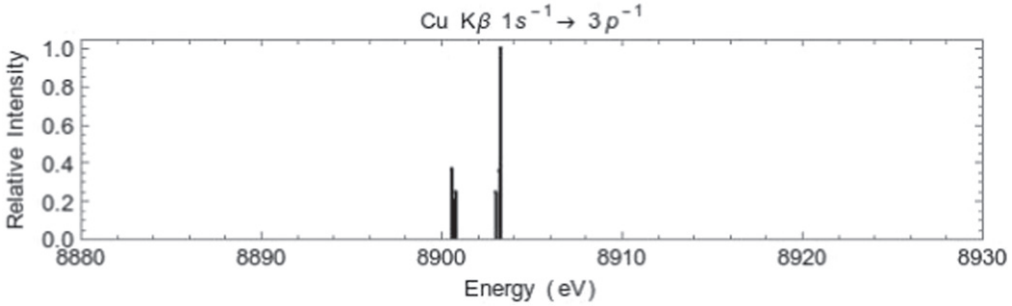

Figure 1. Copper $K\beta$ diagram lines using method 2, by addressing the correct CSFs with dominant contributions to the total ASF.

6. Calculations of copper $K\beta$ satellites

In order to investigate the characteristic profile of copper $K\beta$, in addition to the diagram lines $1s^{-1}\rightarrow 3p^{-1}$, we must also consider the transitions of the satellites due to a removal of an electron from each of the subshells 3d, 3p, 3s and 4s. Double shake from 3d subshell is also potentially significant. We therefore calculate the transitions $1s^{-1}3d^{-1}\rightarrow 3p^{-1}3d^{-1}$, $1s^{-1}3d^{-2}\rightarrow 3p^{-1}3d^{-2}$, $1s^{-1}3p^{-1}\rightarrow 3p^{-1}3p^{-1}$, $1s^{-1}3s^{-1}\rightarrow 3p^{-1}3s^{-1}$, and $1s^{-1}4s^{-1}\rightarrow 3p^{-1}4s^{-1}$. The procedure is similar to the calculations of $K\beta$ transition in the diagram lines presented above, with the ASF serial numbers corrected to indicate the true dominant CSFs in the list. The satellite transition spectra are presented in figure 2.

The GRASP2K version 1.1, RCI4 update was used to solve the DHF equations. The Breit interaction and first order QED were included perturbatively. In generating the CSF basis, single and double excitations were allowed from the 3p, 3d and 4s subshells to virtual orbitals up to the $n = 5$ shell. Core–core and core–valence correlations were ignored. Wavefunctions were optimized individually for both initial and final states, in the same way as optimizing the wavefunctions of the diagram lines.

In figure 2, the stick diagrams demonstrate the transitions of the satellites due to an ionization of one or two electron(s) in 3d, 3p, 3s and 4s subshell, following the sudden removal of the core 1s electron. Each of the sticks represents a transition, and the relative heights between the sticks in each diagram represent the relative intensities of the transitions. The number of CSFs of each satellite transition is of order 10^4. The large number of CSFs made it impossible for calculations in the past literature if the 4s electron was included. The spectra of 3d, $3d^2$, 3p and 3s satellites in figure 2 are similar to those of Deutsch *et al* [12] using DF and HF calculations. However, since the 4s electron has been included, the number of transitions and the relative intensities between the transitions in each satellites are now computed accurately. In our calculations, we also consider the 4s satellite. Our 4s satellite is actually the calculations for the $K\beta_{1,3}$ diagram lines by Deutsch *et al* [12] since the 4s electron was neglected in their

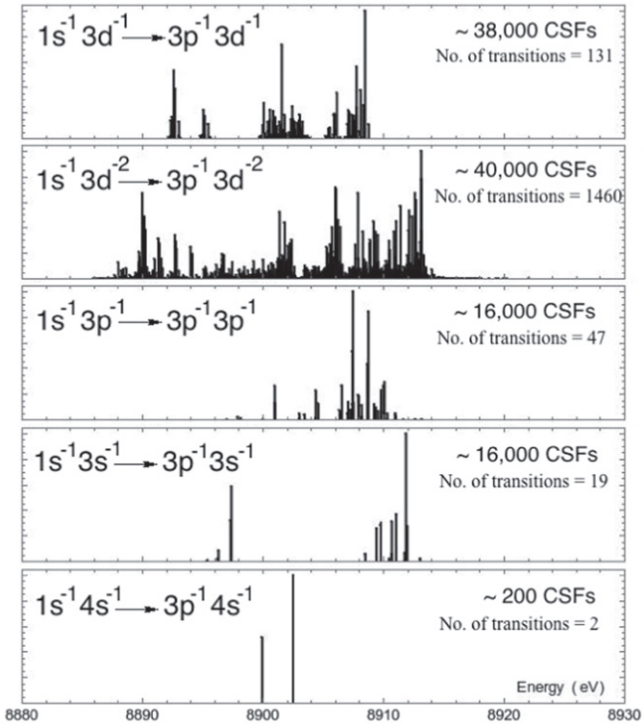

Figure 2. Copper $K\beta$ energy spectra and stick diagrams showing relative intensities. Note the complex multiplets and sub-structure with many transitional energies and CSFs.

calculations. The spectrum of our 4s satellite is almost identical to the diagram line spectrum obtained by Deutsch *et al* [12], in which, the number of transitions is 2, and the intensity ratio between the two lines is approximately 1:2. This implies that our method of calculation(s) is plausible.

7. Shake probabilities in the high energy limit

7.1. Our shake probability calculations using the multi-configuration approach with the sudden approximation

Shake processes have been investigated in many previous works. The sudden approximation in the high energy limit of an electron removed from the atomic orbital has been demonstrated to be a good method to determine shake probabilities when valid [32]. Most available theoretical calculations used the sudden approximation, that is, in the high energy limit, an electron is ionized to the continuum (shake-off) or excited to the higher bound state (shake-up), causing a sudden change in the atomic potential.

The theory of satellites and shake probability calculations have been presented in the literature in the 1960s by [33]. Early calculations of shake probabilities in the high energy limit were done for Ar Kβ by Dyall and Grant [34, 35], using CI wavefunctions based on MCDF-EAL calculations. Our calculations of the shake probabilities are based on [32]. Chantler *et al* have used the multi-configuration method in the sudden limit to calculate the shake probabilities in the 3d subshell in transition metals [4, 36]. In the sudden limit, the initial ionization takes place in a time frame much shorter than orbital relaxation, and the shake-off probability can be expressed as the overlap integral between the wavefunctions of initial and final states.

The neutral atom is initially in an eigenstate of the $N + 1$ electron Hamiltonian, $H(N + 1)$, with an atomic wavefunction $\Psi_{\rm A}(N + 1)$, prior to ionization. If an electron is suddenly removed from an orbital, the wavefunction undergoes the transformation:

$$\Psi_{\rm A}(N + 1) \rightarrow \tilde{\Psi}_A(N) \tag{6}$$

$|\tilde{\Psi}_{\rm A}(N)\rangle$ is the state of the atom before relaxation as soon as an electron is suddenly removed from the 1s subshell. It uses the converged wavefunction of the neutral copper atom (with one 1s electron missing), since the initial assumption is that the ionization of an electron from 1s orbital occurs in the high energy limit such that the wavefunction does not have enough time to adjust itself. Upon relaxation, the wavefunction becomes the $1s^{-1}$ state $|\Psi_B(N)\rangle$. The shake-up or shake off probability, $P_{\rm shake}$, is the probability of the system initially in state $|\tilde{\Psi}_{\rm A}(N)\rangle$ to be found in any state other than $|\Psi_B(N)\rangle$, which can be written as:

$$P_{\rm shake} = 1 - \left| \left\langle \Psi_B(N) \middle| \tilde{\Psi}_{\rm A}(N) \right\rangle \right|^2, \tag{7}$$

where $|\Psi_B(N)\rangle$ and $|\tilde{\Psi}_{\rm A}(N)\rangle$ are the N electron wavefunctions with the same set of quantum numbers.

In the multi-configuration framework, the ASF atomic wavefunctions $|\tilde{\Psi}_{\rm A}(N)\rangle$ and $|\Psi_B(N)\rangle$ are linear combinations of CSF Slater determinants:

$$|\tilde{\Psi}_{\rm A}(N)\rangle = \sum_j c_j |\tilde{\Phi}_{{\rm A}j}\rangle, \text{ and } |\Psi_B(N)\rangle = \sum_k d_k |\Phi_{Bk}\rangle. \tag{8}$$

Equation (7) can be written as:

$$\begin{aligned} P_{\rm shake} &= 1 - \left| \left\langle \Psi_B(N) \middle| \tilde{\Psi}_{\rm A}(N) \right\rangle \right|^2 \\ &= 1 - \left| \sum_j \sum_k c_j d_k \left\langle \Phi_{Bk}(N) \middle| \tilde{\Phi}_{{\rm A}j}(N) \right\rangle \right|^2, \end{aligned} \tag{9}$$

where c_j and d_k are the mixing coefficients of the CSFs, which can be found using the program extmix in GRASP2K. $|\tilde{\Phi}_{{\rm A}j}\rangle = \mathcal{A} \prod_{n\kappa}^{N} |\tilde{\phi}_{{\rm A}jn\kappa}\rangle$ and $|\Phi_{Bk}\rangle = \mathcal{A} \prod_{n'\kappa'}^{N'} |\Phi_{Bkn'\kappa'}\rangle$. The overlap in equation (9) can be written as:

$$\left\langle \Phi_{Bk}(N) \middle| \tilde{\Phi}_{{\rm A}j}(N) \right\rangle = \prod_{n,\kappa}^{N} \prod_{n',\kappa'}^{N} \left\langle \phi_{Bkn'\kappa'} \middle| \tilde{\phi}_{{\rm A}jn\kappa} \right\rangle. \tag{10}$$

We make simplifying assumptions that the shake-up is negligible and the inner-shell photoionization includes only pure shake-off processes. This is valid, given that in the sudden limit, the orbital relaxation is small, and the ionization is dominant over excitation. This has been indicated in theoretical and experimental literature [37–39]. Therefore, shells with different quantum number n and κ have zero overlap, and we can also ignore overlaps of any two wavefunctions with different occupation numbers. The overlap in

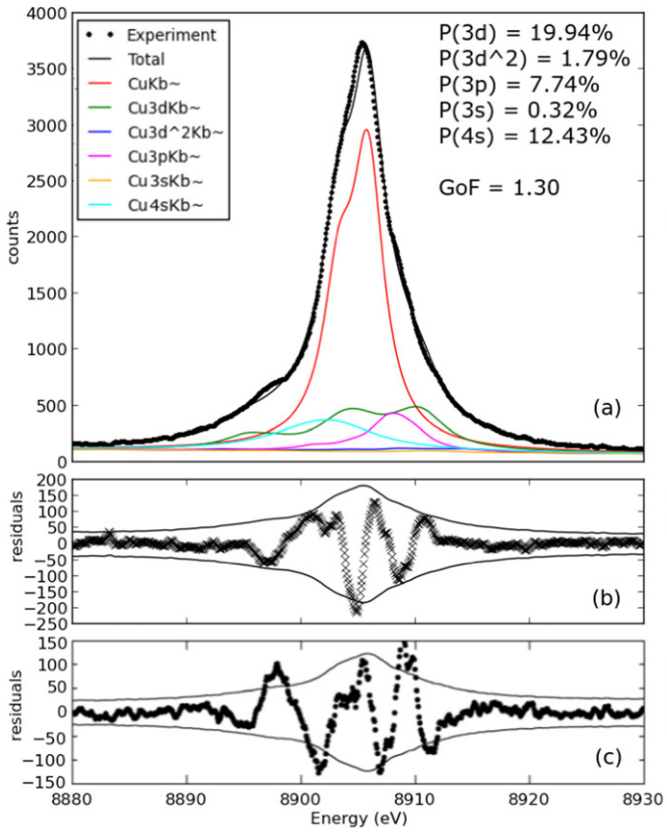

Figure (3.1): shake probabilities are fixed and $\chi^2_{\text{reduced}} = 1.30$ (fit 3).

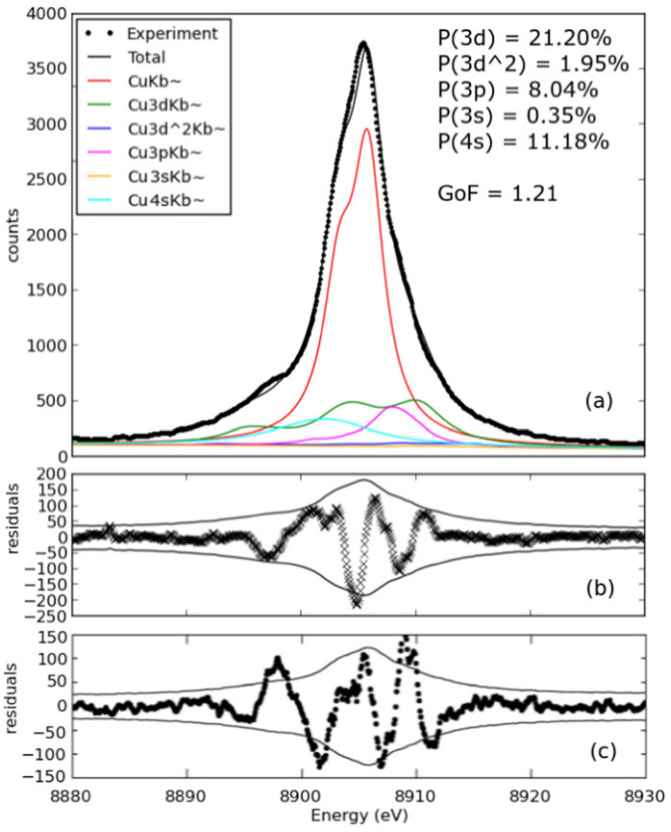

Figure (3.2): shake probabilities as free parameters and $\chi^2_{\text{reduced}} = 1.21$ (fit 9).

Figure 3. Figures (3.1(a)) and (3.2(a)) show the fits of $K\beta_{1,3}$ and the satellites from our *ab initio* MCHDF calculations to the best available experimental data by Deutsch *et al* [14], using the models in fit 3 and fit 9 of table 5. Figures (3.1(b)) and (3.2(b)) show our residuals. Figures (3.1(c)) and (3.2(c)) are the residual plots from Deutsch *et al* [14] by fitting their theoretical results for $K\beta_{1,3}$ and the 3d satellite spectrum with $P_{\text{shake}}(3\text{d}) = 26.0\%$, independent widths and $\chi^2_{\text{reduced}} = 1.36$.

equation (10) can take the values:

$$\left\langle \phi_{Bkn'\kappa'} \middle| \tilde{\phi}_{Ajn\kappa} \right\rangle = 0 \quad \text{for } n \neq n',\ \kappa \neq \kappa' \\ = 1 - \epsilon_{n\kappa} \text{ for } n = n',\ \kappa = \kappa'. \qquad (11)$$

The value $1 - \epsilon_{n\kappa}$ of the overlap of the two wavefunctions can be evaluated from the overlap of the two orbital radial wavefunctions. The GRASP2K program readrwf supplies values of the radial components $P(r)$ and $Q(r)$ on a standard grid, from which the overlap integral of equation (4) can be calculated numerically. The total shake probability from equation (9) can be written as:

$$P^{\text{shake}}_{\text{total}} = 1 - \left| \sum_j \sum_k c_j d_k \prod_{n\kappa} \left\langle \phi_{Bkn\kappa} \middle| \tilde{\phi}_{Ajn\kappa} \right\rangle^{M_{jn\kappa}} \right|^2, \qquad (12)$$

where $M_{n\kappa}$ is the electron occupation number of the wavefunction with quantum number $n\kappa$.

Shake-off probabilities cannot be assigned to individual shells or subshells, but instead, they can only be assigned to the atom. This is because the sets $\{|\tilde{\Phi}_{Aj}\rangle\}$ and $\{|\Phi_{Bk}\rangle\}$ consists of CSFs with differing occupation numbers and the ASF is a combination of a number of electron configurations [32]. However, the calculations of shake probabilities in practice can be approximated by assigning those probabilities to a set of quantum numbers. The calculation of satellite energies generally proceeds by assuming the shake-off electron can be localized to a particular subshell [3, 12, 18, 40]. By assigning the shake probabilities to individual shells or subshells, the results from our calculations are accurate up to the first-order approximation. The procedure of assigning shake-off probabilities to subshells is similar to the recipe by Lowe *et al* [32]. The possibility of an electron shaken from subshell n, κ from equation (7) can be now simplified as:

$$P^{\text{shake}}_{n\kappa} = 1 - \left| \sum_j \sum_k c_j d_k \left\langle \phi_{Bkn\kappa} \middle| \tilde{\phi}_{Ajn\kappa} \right\rangle^{M_{jn\kappa}} \right|^2, \qquad (13)$$

where $M_{jn\kappa}$ comes from the CSF sum of orbitals. The probabilities of the single and double shakes from 3d, 3p, 3s and 4s subshells are calculated using equation (13) and presented in table 3. In this approach, the double shake occurs when the time difference between the removal of two electrons in the same subshell is negligible, insufficient for the potential to re-adjust itself. Therefore the double shake can be approximated as a one-step process when any two indistinguishable electrons are ionized from nl simultaneously.

Table 3. Shake probabilities calculated in this work, using the multi-configuration approach, equation (13). Uncertainties are the correction due to inclusion of third order CSF contributions as discussed in the text.

Shake from	3d	$3d^2$	3p	3s	4s
Probability (%)	19.94 ∓ 0.14	1.79 ∓ 0.04	7.74 ∓ 0.10	0.32 ∓ 0.02	12.43 ∓ 0.15

Table 4. Summary of shake probabilities (in %) from theoretical and experimental results in the literature, and the shake probabilities from our theoretical modelling using the multi-configuration approach in the sudden limit. The empirical fits of experimental data were unable to fit more than just the 3d (dominant) satellite.

	Literature	3d	3p	$3d^2$	3s	4s
Theory	Mukoyama & Taniguchi [41]	9.7	2.5			9.7
	Kochur *et al* [42]	13.0	2.6	0.9		
Experiment	Galambosi *et al* [37]	26.2				
	Holzer *et al* [43]	18.5				
	Diamant *et al* [38]	25.0				
	Enskinsch *et al* ($K\beta$) [44]	29.0				
	Ito *et al* [45]	23.1				
	Deutsch *et al* [39]	29.0				
	Deutsch *et al* ($K\beta$) [39]	26.0				
	Chantler (2009) *et al* [2]	26.0				
	Chantler (2012) *et al* [4]	39.0				
Theory	This work	19.9	7.7	1.8	0.3	12.4

Let $\mathcal{M}^{n\kappa}$ be a matrix with each element $\mathcal{M}^{n\kappa}_{jk} = c_j d_k \left\langle \phi_{Bkn\kappa} | \tilde{\phi}_{\mathrm{A}jn\kappa} \right\rangle^{M_{jn\kappa}}$. In order to calculate the shake probability $P^{\mathrm{shake}}_{n\kappa}$ in equation (13), we need to sum up all the matrix elements of $\mathcal{M}^{n\kappa}$. This is difficult since the number of CSFs in each list is of order 10^4. Therefore, we only consider CSFs with significant contributions to the ASF. Each of the sums in equation (13) is no longer expanded to the total number of CSFs in the CSL, instead, it will only expand to the second order. The first order expansion includes the single CSF with the dominant contribution to the ASF (about 96.5%), while the second order expansion includes up to 100 or so CSFs with mixing coefficients c_j or d_k of order 10^{-2}, depending upon which satellite is involved.

The shake probabilities reported in table 3 are calculated using equation (13) to the second order in the expansion of CSFs. The uncertainties are estimated from the higher-order (i.e. third order) corrections of the shake probabilities, from perhaps hundreds of CSFs with lower mixing coefficients, which tend to decrease the shake probabilities with the expansion of the CSFs. Therefore, the uncertainties of the shake probabilities are labelled with the $\mp$ symbols.

7.2. Shake probability calculations compared with the theoretical and experimental literature

7.2.1. Theoretical literature. For many-electron atoms, Mukoyama and Taniguchi [41] followed Carlson and Nestor's treatment [46] to calculate the shake-off probability P_{nl}:

$$P_{nl} = 1 - \left| \int \psi'^{*}_{nl} \psi_{nl} \mathrm{d}\tau \right|^{2N} - P_{\mathrm{F}} \qquad (14)$$

where ψ_{nl} and ψ'_{nl} are the wavefunctions of the neutral atom and the ion with a single vacancy in the inner shell, respectively. N is the number of electrons in the nl shell, and P_{F} is probability of the forbidden transitions. Our formalism of shake probabilities calculation in equation (7) follows the same logic as that used by Mukoyama and Taniguchi in equation (14).

Kochur *et al* [42] did not calculate absolute shake probabilities, but instead computed shake probabilities relative to the probability of $K\beta_{1,3}$ transitions. The single and double shake probabilities from the shell nl, relative to the diagram lines were

$$P_{\text{single shake}} = N_{nl}\left(\left\langle \tilde{\phi}_{nl} \middle| \phi_{nl} \right\rangle^{-2} - 1 \right), \qquad (15)$$

$$P_{\text{double shake}} = \frac{1}{2} N_{nl}\left(N_{nl} - 1\right)\left(\left\langle \tilde{\phi}_{nl} \middle| \phi_{nl} \right\rangle^{-2} - 1 \right)^2, \qquad (16)$$

where $\left\langle \tilde{\phi}_{\mathrm{nl}} | \phi_{nl} \right\rangle^{-2} - 1$ is the probability of shake from the subshell nl upon $n_0 l_0$-ionization per N_{nl}-electron [42]. The factor $\frac{1}{2} N_{nl}(N_{nl} - 1)$ is the combinatorics term, associated with the probability of having two random electrons removed in the total N_{nl} electrons of the subshell simultaneously. This follows similar logic to equations (7) (13) and (14) but with a Taylor expansion to first order.

While the formalism of these approaches and computations appears consistent, the results, possibly due to issues of wavefunction convergence and completeness, vary by more than a factor of two (table 4). In some cases this can be due to the computation of some related parameter such as a computation of amplitude coefficient rather than probability [4].

7.2.2. Experimental literature. The determination of the shake probabilities from the experimental spectra may proceed by fitting the theoretical profiles of the diagram

lines $K\beta_{1,3}$ and satellites to the experimental results; or by fitting a series of Lorentzians to the experimental spectra or phenomenological fitting.

One of the earliest studies was done by Deutsch *et al* [12]. The instrumental function in the double crystal spectrometer was very narrow so that no broadening for finite resolution was necessary. Fits were done using the measured and smoothed data. The 3d shake probabilities reported [12, 39] were 29% and 26% respectively for copper $K\alpha$ and $K\beta$. Galambosi *et al* [37] used multi-configuration fits to study the shake probability in the copper $K\alpha$ transition, however with the excitation energies near the threshhold. The value found in this study is 25% ± 2%, including both shake-up and shake-off processes [37]. This result is in good agreement with the value found by Diamant *et al* [38] of 25%. Similarly, the 3d shake-off probability calculated by Enskisch [44] for $K\beta_{1,3}$ and $K\beta_{2,5}$ spectra were found to be 30% and 29% respectively. The 3d shake probabilities found by Chantler *et al* (2009 and 2012) are both from the fitting of theoretical calculations of copper $K\alpha$ from a MCDHF approach to the best available experimental data [14]. The 4s electron was neglected in [2], but was included in the calculations in [4]. The discrepancies between these two results by Chantler *et al* and other experimental results are partly due to: only including 3d satellite; differences in the theoretical calculations and convergence of wavefunctions; and the strong correlation between different fitting parameters.

Most of the calculations have been done on copper $K\alpha$. Because the ionization event, if sudden, is meant to precede the relaxation from either subshell, the shake and satellite probabilities should ideally be consonant. However, theoretically there can be issues of detailed wavefunction convergence and orthogonalization; and experimentally the limited resolution of Kβ transitions can preclude clear determination of satellite components and magnitudes. The values for the $K\beta$ transition can be found in the papers by Deutsch *et al* [12, 14, 43] and Enkisch *et al* [44]. It is unclear whether Mukoyama and Taniguchi [41] and Kochur *et al* [42] modelled their computations upon $K\alpha$ or $K\beta$. As stated, this should not affect the results. The discrepancies between the theoretical calculations and the experimental results therefore remain unclear. One contribution is certainly due to fitting only a single satellite component (e.g. 3d) to unresolved spectral components.

From table 4, our 3d shake probability from the multi-configuration approach are in moderate agreement with the experimental values by Holzer *et al* [43] and Ito *et al* [45]. Our 3d shake calculation is much smaller than most of the semi-empirical values. This might be because only the 3d shake was modelled in the experimental literature, and therefore, those probabilities were overestimated.

Our calculations reveal considerably higher probabilities of shake processes, compared to the theoretical calculations done by Mukoyama and Taniguchi [41] and Kochur *et al* [42] especially for the single electron shake from 3d and 4s subshells, and the double shake from the 3d subshell. The shake probabilities calculated in this work are, however, consistent with the results by Chantler *et al* (2010) [3].

8. Modelling, analysis and assumptions

8.1. Fitting parameters and uncertainties using least-squares analysis and Bayesian constraints

Experimental data was obtained from a meticulous double crystal laboratory-based spectrometry experiment [14]. The authors stated that the instrumental and thermal broadening were negligible. Therefore, Gaussian width σ can be set to be zero, and our broadening function becomes a Lorentzian profile. The results of MCDHF calculation for the diagram lines, or for each set of satellites, can be presented by a 'stick diagram', with each vertical line represents a transition with energies and intensities calculated from GRASP2K, but with no width. To represent a transition we convolve each component in the 'stick' diagrams with a broadening function. The convolved peaks are then fitted to experimental data to determine the intensity of the diagram lines, the intensity of each set of the satellites, as well as transition widths [2, 3, 47]. An overall offset and scale of energy may result from the calibration of the experiment. On the other hand, each set of diagram or satellite lines may be subject to a different energy offset due to limitations in the accuracy of the theoretical convergence.

Consequently, fitting parameters include the full width at half maximum, the energy offset between experimental calibration and theoretical convergent prediction, and the probability of each of the diagram lines and each satellite spectrum for a maximum total of 17 possible independent parameters (table 5). However, from our theoretical modelling, we are able to constrain all of the satellite probabilities, all the component spectral distributions, common widths for the $K\beta$ diagram components, for a total of 12 independent parameters given Bayesian physical constraints. Of course, with a number of the fitted models involving subsets of the computed satellites, the number of free parameters were much smaller, but these were more akin to exemplars of the degree of convergence and robustness towards physical models.

8.2. New theoretical calculations and predictions compared with the theoretical literature

In this study, not only 3p, 3s and 4s satellites are fitted and reported, but energy offsets and fitting uncertainties are also reported. To investigate the potential value of our new approach, a fitting procedure is implemented with fixed parameters derived from our theory and prior literature. The widths and offsets are always free parameters, which are fitted to the experimental spectrum to obtain goodness-of-fit χ^2_{reduced}. The energy of each transition line and its intensity are taken from our calculations for the diagram and each set of satellites. Hence there are *a priori* constraints as to the detailed substructure of each diagram or satellite spectrum, and also as to the shake probability dictating their amplitude,

Table 5. Fits to the best available experimental spectrum of copper $K\beta$ [14].

Fit	(1) M&T	(2) Kochur *et al*	(3) Multi-config equation (13)	(4) 3d	(5) 3d+3p	(6) 3d+4s	(7) 3d+3d^2+4s	(8) 3d+3p+4s	(9) 3d+3d^2+3p 3s + 4s
3d prob. (%)	9.70	12.96	19.94(21)	33.19(40)	34.11(49)	23.86(14)	23.79(29)	23.56(13)	21.20(32)
3d^2 prob. (%)	—	0.80	1.79(04)	—	—	—	1.98(03)	—	1.95(11)
3p prob. (%)	2.46	2.15	7.74(10)	—	7.21(14)	—	—	7.83(26)	8.04(26)
3s prob. (%)	—	—	0.32(02)	—	—	—	—	—	0.35(04)
4s prob. (%)	9.67	—	12.43(14)	—	—	10.01(19)	10.09(16)	10.82(18)	11.18(16)
$\beta_{1,3}$ width (eV)	4.56(02)	4.83(03)	3.29(03)	3.87(04)	3.42(03)	3.94(03)	3.79(03)	3.30(02)	3.25(02)
3d width (eV)	2.58(14)	3.14(02)	4.87(17)	5.81(03)	6.82(09)	4.66(13)	4.40(09)	5.56(19)	4.99(18)
3d^2 width (eV)	—	3.55(47)	3.05(56)	—	—	—	4.39(44)	—	3.18(32)
3p width (eV)	6.57(68)	5.72(15)	3.23(07)	—	3.45(18)	—	—	3.03(17)	3.21(12)
3s width (eV)	—	—	3.17(40)	—	—	—	—	—	5.60(48)
4s width (eV)	9.51(03)	—	8.99(05)	—	—	9.57(06)	9.33(07)	8.99(03)	9.18(06)
$\beta_{1,3}$ shift (eV)	2.84(01)	2.68(01)	2.60(01)	2.67(01)	2.50(01)	2.74(00)	2.70(00)	2.60(01)	2.58(01)
3d shift (eV)	2.44(01)	2.53(02)	2.60(02)	2.17(04)	1.94(04)	2.49(03)	2.45(03)	2.60(03)	2.48(05)
3d^2 shift(eV)	—	2.63(32)	2.60(11)	—	—	—	2.67(37)	—	2.58(47)
3p shift (eV)	2.74(05)	0.49(11)	0.10(04)	—	0.02(02)	—	—	0.18(05)	0.02(04)
3s shift (eV)	—	—	0.10(20)	—	—	—	—	—	0.01(24)
4s shift (eV)	0.46(04)	—	0.46(10)	—	—	1.50(05)	1.61(06)	0.20(11)	0.28(07)
Total peak (eV)	8905.65(80)	8905.48(68)	8905.69(79)	8905.69(41)	8905.62(55)	8905.69(29)	8905.69(68)	8905.70(45)	8905.69(93)
χ^2_{reduced}	2.18	2.32	1.30	1.30	1.30	1.40	1.37	1.32	1.21

Parameters constrained to zero fit are indicated with '-'. The fixed parameters in fits (1–3) are the shake-off probabilities, as *a priori* constraints from Mukoyama and Taniguchi (M & T, column 2) [41], from Kochur *et al* (column 3) [42], and from our multi-configuration approach (multi-configuration, equation 13, column 4). In fits (4–9) all the parameters are free parameters with a varying set of fitted satellites. The consistency between fits using the shake probabilities as constraints from our theory (fit 3) and the empirical fit of the best available experimental data allowing these as free parameters (9) is remarkable.

following the usual Bayesian hypothesis, for the first three fits in table 5. While widths (natural and instrumental broadening) and energy offsets between theoretical eigenvalues and experimental positions are in general fully free, one can consider the likely physical basic of the resulting fitted values within their uncertainties.

Fit (1) uses the shake-off probabilities of 3d, 3p and 4s satellites obtained by Mukoyama and Taniguchi [41]. The maximum energy offset for the diagram lines is large: 2.84 eV. The goodness of fit (1) is relatively poor ($\chi^2_{\text{reduced}} = 2.18$).

Similarly, using the shake probabilities from Kochur *et al* [42] in fit (2), the goodness-of-fit is poorer ($\chi^2_{\text{reduced}} = 2.32$).

In fit (3), the shake probabilities are calculated using our multi-configuration approach equation (13). The maximum energy offset corresponds to the offset of the diagram lines, which is 2.60 eV. The χ^2_{reduced} is very close to unity (1.30). This demonstrates our theoretical calculations of shake-off probabilities, using the multi-configuration approach, may be in excellent agreement with the experiment.

8.3. Discussion of free parameter modelling of the experimental spectrum and comments on the theoretical prediction

In fits (4–6), all the parameters, including shake probabilities, linewidths, and energy shifts, are set free. 3d shake is fitted in all the fits, since this is the dominant contribution to the total spectrum, as indicated in our theoretical calculations and from both the theoretical and experimental literature.

In fit (4), only 3d shake is taken into consideration. The uncertainties of the fitted parameters and the difficulty of the fitting procedure can be minimized due to a small number of free parameters. Fit (4) implies a significantly high 3d shake probability, and this result argrees with other semi-empirical fits in the literature [2, 12, 44]. The significantly higher probability of 3d shake can be explained since 3p and 4s contribution are not fitted. Hence the available and fitted satellite attempts to fill all the asymmetry and gaps not accounted for by the diagram lines.

The Deutsch *et al* modelling [12] used a set of diagram and 3d spectral components, and was a ground-breaking advance, but had independent widths for each diagram line (ours are constrained as dominated by instrumental broadening) and omitted the 4s electron so therefore produced a distinct satellite structure. Perhaps more significantly, this omission of fitting other satellites (which they indeed discuss in their paper) leads to amplification of 3d fitted contributions but a higher χ^2_r. In fit (5) both the 3d and 3p satellites are fitted. Both the χ^2_{reduced} value and the 3d shake probability are similar to those in fit (4). The fitted 3p probability is high compared to the values found in the literature, but is in great support of our theoretical calculation.

Fit (6) implies a relatively high contribution of the 4s shake (10.01 %). The goodness-of-fit value in fit (5) is the result of the correlation between the parameters. We expect that the 4s shake probability has high uncertainty because the 4s satellite spectrum is almost identical (and therefore degenerate) to the spectrum of the diagram lines. In fact, our 4s satellite spectrum was defined as the diagram transition in the *ab initio*s calculation by Deutsch *et al* [12]. Therefore, it is difficult to separate the spectrum of 4s satellite (and the independent probability) from the diagram line.

In fit (7), 3d, $3d^2$ and 4s satellites are fitted. In fit (8), 3d, 3p and 4s satellites are fitted. The 3d and 4s probabilities found in both fits are highly consistent with each other, and are in fair agreement with our theoretical calculations. Both the $3d^2$ and 3p probabilities agree with the prediction very well.

The degeneracy of the 4s satellite spectrum compared with the diagram line spectrum decreases the number of degrees of freedom and increases the strongly correlated parameters without any improved fit. Therefore, when including 4s satellite in the fitting, fits (6–8) yield higher values of χ^2_{reduced} compared to fits (4–5). By comparing χ^2_{reduced} values between fits (5–8), the best fits are sensitive to 3p shake probability. The 3p satellite including in the fitting improves the goodness of fit significantly. On the other hand, in fit (8), the χ^2_{reduced} is only slightly larger than that of fits (3–5).

It is remarkable that the fitted shake probabilities of $3d^2$, 3p and 3s satellites, indeed, are highly consistent with our predicted values using the multi-configuration approach. In fit (9), all the satellites 3d, $3d^2$, 3p, 3s and 4s are taken into consideration. All fitted values are within 10% of the theoretical calculations. The results are significant considering a large number of free parameters are strongly correlated with each other, resulting in larger uncertainties. The 3d shake probability is found to be slightly higher than expected from our multi-configuration calculations. On the other hand, the 4s shake probability is found to be slightly smaller than predicted. This, again, may be due to the strong correlation between the free parameters, and due to the significant overlap between the 4s and the satellite spectrum. Moreover, since the contributions from both the 3d and 4s satellites are high, the discrepancies between the fitted 3d and 4s shake probabilities in fit (9) and the values from the theoretical calculations are not significant.

In each fit, if a parameter is fixed and varied toward its value indicated in table 5, it is observed that the χ^2_{reduced} converges to the same value in the table. This is to ensure our fitting procedure yields a robust fit converging to the true minimum, with parameters constrained to physical values. This remarkably appears to agree with the shake modelling when 3p and $3d^2$ satellites are included with both the diagram lines and 3d satellite.

The remarkable consistencies between results from the theory and the semi-empirical fits are the result from our *ab initio* multi-configuration method. Our method demonstrates not only excellent convergence of the wavefunctions of both the diagram and the satellites, and of the accuracies of the transition energies and relative intensities, but also the validity of the formalism of the shake probability calculations in the sudden limit. Table 5 demonstrates that not only the

Table 6. Fitted linewidths compared to the literature.

	Theory			Experiment			This work	
Width (eV)	McGuire [49]	Yin *et al* [48]	Crasemann & Chen [12]	Deutsch *et al* [12]	LaVilla [25]	Yin *et al* [48] [50]	Theory (fit 3)	Semi-empi -rical (fit 9)
$K\beta_1$	6.66	3.51	4.90	4.08	3.52	2.48	3.29	3.25
$K\beta_3$	6.66	3.51	5.00	4.60	3.52	3.55	3.29	3.25
3d satellite				4.88			4.87	4.99
$3d^2$ satellite							3.05	3.18
3p satellite							3.23	3.21
3s satellite							3.17	5.60
4s satellite							8.99	9.18

'Theory' represents the use of theoretical shake probabilities as fixed parameters, fitted to the experimental data to obtain linewidths. The consistency is reasonable.

fitting parameters in the semi-empirical fits are highly consistent with each other, but they are also consistent with the theoretical calculations using the multi-configuration approach. This shows a high level of internal consistency in our theoretical and semi-empirical methods. In addition, the quality of the fits implies that our theoretical calculations are in excellent agreement with the experiment.

8.4. Investigation of theory using experimental data for the widths and amplitudes

Further investigation is required in order to confirm the validity of our theoretical model and assumptions. That is, how accurate are our theoretical predictions of satellite probabilities and of the spectral amplitudes in relation to the latest available experimental data?

We can compare the transition parameters in our theoretical and semi-empirical values to the values available in the literature. The peak of the $K\beta$ spectrum measured by Bearden and Shaw [27] is at 8905.52 eV, and by Deutsch *et al* [14] is at 8905.42 eV. Our total spectrum peak obtained in table 5: 8905.69 ± 0.93 eV, agrees well with the literature values. Our results demonstrate good quality of fits and a high degree of consistency with theoretical predictions.

Table 6 shows the transition widths of the diagram and 3d satellites obtained in previous theoretical and experimental works. The linewidths in our fits are strongly correlated to each other, therefore, it is not easy to determine the values accurately, and it is difficult to compare with the literature. We cannot compare our results directly with the literature values since the $3d^2$, 3p, 3s and 4s shakes were not fitted in the literature. However, the consistency between our values of the linewidths of the diagram and the 3d satellite transitions and the literature values is remarkable. The widths of our diagram lines in fits (3) and (9) are in fair agreement with the experimental values by LaVilla [25], and with the theoretical values by Yin *et al* [48]. The widths of our 3d satellite are also in very good agreement with [12]. Hence, we can conclude that our final results using either fits (3) or (9) are physical and plausible within the uncertainties determined in the fits.

8.5. Comments on the energy offsets

From the fits in table 5, the energy spectra of the diagrams and the satellites have to be shifted to align with the experimental data by different amounts as seen in [12] to fit the values from the *ab intio* DHF calculations to the values from the double crystal experiment. The offsets of the diagram and the 3d satellite spectra are comparable to the values obtained by Deutsch *et al* [12]. The $3d^2$ spectrum is also shifted by approximately the same amount. On the other hand, the spectra of 3p, 3s and 4s satellites are only slightly shifted. The 0.82 eV difference in the transition energy of the diagram lines between method 1 and method 2 suggests a theoretical convergence issue at around this level. This is the main empirical fitting parameter left in our theoretical computations. Uncertainties in the fitting may also cause different individual energy offsets, and uncertainties of transition energies may be underestimated. The differences in the energy offsets of the satellites therefore require further analysis. Analysis of the experimental calibration is also needed relating to this question. Many might consider that these shifts are quite small compared to the widths, and hence that they are plausible within experimental calibration uncertainty and theoretical convergence. This may in fact be the case.

9. Conclusion

In this study we have presented a complete theoretical characterization and analysis of the $K\beta$ x-ray emission profile of copper. Using the MCDHF approach implemented in the latest version of the relativistic atomic theory package, GRASP2K version 1.1 with the improved self-energy screening of RCI4, we are able to explain the $K\beta$ transitions in a complex open-shell many-electron atomic system. The diagram lines $\beta_{1,3}$ and a full set of potentially significant spectator vacancies are also studied quantitatively.The results from the MCDHF demonstrate not only excellent convergence in transition energies up to 0.01 eV, but also the gauge invariant wavefunctions (to 0.6%). Peak separations converge to the third significant figure, while component ratios β_3 : β_1 are convergent to the fourth significant figure.

The results from our MCDHF are remarkable, since the total number of CSFs in our calculations exceeds 10^5 and the number of transition components is of order 1500.

We have successfully calculated the probabilities of single and double shake processes in 3d, 3p, 3s and 4s orbitals, which account for the broad, asymmetric peak of copper $K\beta$. In most cases these theoretical computations yield an uncertainty of 0.1%–0.15% (measured by the convergence from including higher order CSF contributions—the systematic uncertainty is undoubtedly larger than this but difficult to evaluate meaningfully). However other theoretical and experimental works have derived shake probabilities in the same impact or sudden limit discrepant by many times this uncertainty, usually due to the difficulty of empirically fitting a spectrum with insufficient components, the difficulty of evaluating the correlated fitting space, or the limitations of the theoretical computations. This is at some level proven by the improved χ^2_{reduced} fits using our theoretical shake probabilities, and the consistency of the empirical experimental fits of the shake probabilities to our theoretical values to within about 5% of the relevant shake probability, or about 1% of the transition probability.

Different free experimental fits have also been done to calculate shake probabilities, linewidths and energy offsets of 3p, $3d^2$, 3s and 4s satellites for the first time. The goodness-of-fit values of both the theoretically constrained and free experimental fits are remarkably close to unity, implying a robust fitting procedure. Our theoretical values strongly agree with the experimental free fits, and the results from our own free fits to the best available data are also in remarkable agreement. This implies a high degree of internal consistency between our theory and experiment. The results from our study represent a significant improvement not only on the computational techniques, but also of the methodology and analysis. Our theoretical method using the multi-configuration approach demonstrates the potential capability of resolving current discrepancies between the theoretical and experimental results.

Further work will be required to understand the pattern of satellite energy offsets, but this could lie in eigenvalue convergence of the complex open-shell, inner-shell processes. Further study of characteristic radiation will also be required to gain more complete understanding of the satellite transitions and small but potentially significant energy offsets and to resolve further discrepancies between theory and experiment.

References

[1] Markowicz A A 2001 *Handbook of X-Ray Spectrometry* ed R V Grieken and A A Markowicz (Boca Raton, FL: CRC Press) chap 1

[2] Chantler C T, Hayward A C L and Grant I P 2009 *Phys. Rev. Lett.* **103** 123002

[3] Chantler C T, Lowe J A and Grant I P 2010 *Phys. Rev.* A **82** 052505

[4] Chantler C T, Lowe J A and Grant I P 2012 *Phys. Rev.* A **85** 032513

[5] Grant I P 1974 *J. Phys. B: At. Mol. Phys.* **7** 1458–75

[6] Grant I P 1988 *Methods in Computational Chemistry* ed S Wilson (Berlin: Springer) pp 1–71

[7] Chantler C T, Nguyen T V B, Lowe J A and Grant I P 2014 *Phys. Rev.* A **90** 062504

[8] Jönsson P, Gaigalas G, Bieron J, Fischer C F and Grant I P 2013 *Comput. Phys. Commun.* **184** 2197–203

[9] Carlson T A, Nestor C W, Tucker T C and Malik F B 1968 *Phys. Rev.* **169** 27–36

[10] Roy M, Lindsay J D, Louch S and Gurman S J 2001 *J. Synchrotron Radiat.* **8** 1103–8

[11] Mårtensson N *et al* 2013 *J. Phys.: Conf. Ser.* **430** 012131

[12] Deutsch M, Hölzer G, Härtwig J, Wolf J, Fritsch M and Förster E 1995 *Phys. Rev.* A **51** 283–96

[13] Fischer C F 1987 *Comput. Phys. Commun.* **43** 355–65

[14] Deutsch M, Forster E, Holzer G, Hartwig J, Hämäläinen K, Kao C C, Huotari S and Diamant R 2004 *J. Res. Natl Inst. Stand. Technol.* **109** 75–98

[15] Jönsson P, He X, Fischer C F and Grant I P 2007 *Comput. Phys. Commun.* **177** 597–622

[16] Nguyen T V B, Lowe J A, Pham T L H, Grant I P and Chantler C T 2015 private communication (www.ph.unimelb.edu.au/chantler/opticshome/softwarepackagedownloads.html#GRASP2KRCISE)

[17] Grant I P 2007 *Relativistic Quantum Theory of Atoms and Molecules: Theory and Computation* (New York: Springer)

[18] Lowe J A, Chantler C T and Grant I P 2010 *Phys. Lett.* A **374** 4756–60

[19] Chantler C T, Nguyen T V B, Lowe J A and Grant I P 2013 *Astrophys. J.* **769** 84

[20] Nguyen T V B, Chantler C T, Lowe J A and Grant I P 2014 *Mon. Not. R. Astron. Soc.* **440** 3439–43

[21] Huang K, Aoyagi M A, Chen M H, Crasemann B and Mark H 1976 *At. Data Nucl. Data Tables* **18** 243–91

[22] McAlister A J, Cuthill J R, Dobbyn R C, Williams M L and Watson R E 1975 *Phys. Rev.* B **12** 2973–83

[23] Fuggle J C and Mårtensson N 1980 *J. Electron Spectrosc. Relat. Phenom.* **21** 275–81

[24] Scofield J H 1974 *At. Data Nucl. Data Tables* **14** 121–37

[25] LaVilla R E 1979 *Phys. Rev.* A **19** 717–20

[26] Bremer J and Sorum H 1979 *Phys. Lett.* A **75** 47–9

[27] Bearden J A and Shaw C H 1935 *Phys. Rev.* **48** 18–30

[28] Madden H H, Zehner D M and Noonan J R 1978 *Phys. Rev.* B **17** 3074–88

[29] Bruhn R, Sonntag B and Wolff H W 1979 *J. Phys. B.: At. Mol. Opt. Phys.* **12** 203

[30] Herman F and Skillman S 1963 *Atomic Structure Calculations* (Englewood Cliffs, NJ: Prentice Hall)

[31] Misra U D, Sah M and Gokhale B G 1992 *J. Phys. B: At. Mol. Opt. Phys.* **25** 4107

[32] Lowe J A, Chantler C T and Grant I P 2011 *Phys. Rev.* A **83** 060501

[33] Åberg T 1967 *Phys. Rev.* **156** 35

[34] Dyall K G and Grant I P 1984 *J. Phys. B: At. Mol. Phys.* **17** 1281

[35] Dyall K G 1983 *J. Phys. B: At. Mol. Phys.* **16** 3137

[36] Chantler C T, Lowe J A and Grant I P 2013 *J. Phys. B: At. Mol. Opt. Phys.* **46** 015002

[37] Galambosi S, Sutinen H, Mattila A, Hämäläinen K, Sharon R, Kao C C and Deutsch M 2003 *Phys. Rev.* A **67** 022510

[38] Diamant R, Huotari S, Hämäläinen K, Kao C C and Deutsch M 2000 *Phys. Rev. Lett.* **84** 3278–81

[39] Deutsch M, Gang O, Hämäläinen K and Kao C C 1996 *Phys. Rev. Lett.* **76** 2424–7

[40] Anagnostopoulos D F, Sharon R, Gotta D and Deutsch M 1999 *Phys. Rev.* A **60** 2018

[41] Mukoyama T and Taniguchi K 1987 *Phys. Rev.* A **36** 693–8

[42] Kochur A G, Dudenko A I and Petrini D 2002 *J. Phys. B.: At. Mol. Opt. Phys.* **35** 395–9
[43] Hölzer G, Fritsch M, Deutsch M, Härtwig J and Förster E 1997 *Phys. Rev.* A **56** 4554–68
[44] Enkisch H, Sternemann C, Paulus M, Volmer M and Schülke W 2004 *Phys. Rev.* A **70** 022508
[45] Ito Y, Tochio T, Oohashi H and Vlaicu A 2006 *Radiat. Phys. Chem.* **75** 1534–7
[46] Carlson T A and Nestor C W 1973 *Phys. Rev.* A **8** 2887–94
[47] Illig A J, Chantler C T and Payne A T 2013 *J. Phys. B.: At. Mol. Opt. Phys.* **46** 235001
[48] Yin L I, Adler I, Tsang T, Chen M H, Ringers D A and Crasemann B 1974 *Phys. Rev.* A **9** 1070–80
[49] McGuire E J 1972 *Phys. Rev.* A **5** 1043–7
[50] Krause M O and Oliver J H 1979 *J. Phys. Chem. Ref. Data* **8** 329–38